Chapter 7: The "Fermi Surface Complexity Factor" and Band Engineering using *Ab-Initio* Boltzmann Transport Theory

7.1 - Introduction:

The calculation of electronic and thermoelectric properties from electronic band structure has received much attention lately with the increasing availability of computational algorithms and resources. *Ab-initio* calculations are very important from a materials' design perspective in that they provide insight into the underlying electronic states which give rise to the experimentally measurable thermoelectric properties. However, the correlation between calculated properties and experimental results is usually qualitative at best. Therefore, it is important to understand the methods that experimentalists use to characterize the thermoelectric performance, specifically in the context of what the results indicate about the electronic band structure. In this chapter, I develop a new metric for determining the viability of thermoelectric materials whose electronic band structures have been computed using *ab-initio* techniques. The approach is rooted in the Boltzmann transport equation, but is based on semi-empirical band engineering models and techniques which have been discussed in detail in this thesis (Single Parabolic Band model, Chapter 2). I will also give examples where band engineering (and degeneracy) simply cannot capture the behavior, which is most often observed in systems where additional topological features (in addition to individual isolated carrier pockets) arise. I apply the technique over a large database of compounds to show its validity in high-throughput screening of thermoelectric materials, allowing computations to overcome the limitations of the constant relaxation time approximation (CRTA).

One of the primary modes of improving thermoelectric materials as described in this thesis is through band engineering and carrier concentration tuning, which are often explained using the SPB model where the material properties are assumed to be described by a "free electron"-like band which has a certain effective mass (m_S^*). In terms of the thermoelectric figure of merit, zT, the optimum value can be found to scale with the quality factor (assuming acoustic phonon scattering, "APS"), $B_{APS} = \frac{2k_B^2\hbar}{3\pi}\frac{N_v C_l}{m_c^* E_{def}^2 \kappa_L} T$ (Equation 2-6) [18]. Of the parameters in *B*, the valley degeneracy (N_v) has been shown to be critical for improving zT and has been a theme of this thesis (Chapter 4, 6) [16, 26, 132, 169, 170].

7.2 - Theory

7.2a - Effective Valley Degeneracy (N_v^*)

The valley degeneracy, N_v, is defined as the number of distinct Fermi surfaces that exist at the Fermi level. The origin of these degeneracies can be broken down into two parts: $N_v = N_{v,symmetry} N_{v,band}$, where $N_{v,symmetry}$ is related to the degeneracy of a given point in the Brillouin zone and $N_{v,band}$ is the number of individual bands that are converged at that energy. Valley degeneracy manifests itself by increasing the density of states effective mass, $m_d^* = N_v^{2/3} m_b^*$, relative to the single valley effective mass (m_b^*). This is beneficial for the thermoelectric properties because each individual pocket conducts in parallel while the overall Fermi level does not rise too quickly (allowing the material to simultaneously maintain a high Seebeck coefficient and high mobility). In order to maximize N_v, a highly symmetric Brillouin zone (usually found in high symmetry materials) with band extrema that exist at low symmetry points lead to the highest degeneracy. As described in Figure 7-1, for PbTe and other IV-VI materials, the primary valence band exists at the L-point with $N_{v,symmetry}$=4, and a $N_{v,band}$=1, and a secondary along the Σ line with a high degeneracy of $N_{v,symmetry}$=12, and a $N_{v,band}$=1.

While many semiconductors have their band extrema at the Γ point (the point of highest symmetry in the Brillouin zone), this point only has a $N_{v,symmetry}$ of 1 (although some have multiple degenerate bands, $N_{v,band}$>1). The lead chalcogenides, on the other hand, have their primary valence band (and conduction band) at the *L*-point with $N_{v,symmetry} = 4$ and a secondary valence band along the Σ line, which shows high degeneracy of 12 (see Figure 7-1a). While utilizing the first Brillouin zone's symmetry to simply count the number of degenerate valleys for a given material's primary band is useful for determining whether multiple Fermi surfaces might benefit the thermoelectric performance, it is not always clear how to quantify how much nearby bands contribute. Because electron transport is dominated by charge carriers with energies within a few k_BT of the Fermi level, additional bands must be in this range to lead to zT enhancement: for example, if E_F is well within the first L-band, but is more than a few k_BT from the Σ band, then the transport properties will only reflect that of the L-band (as we observed for low carrier concentrations in SnTe—Chapter 4).

In this thesis chapter, I develop a metric that can serve as an estimate of valley degeneracy in the regions where multiple bands participate in conduction. The "effective valley degeneracy", N_v^*, describes the Fermi level-dependent valley degeneracy in order to estimate the benefit to thermoelectric properties (and quality factor, B) as a result of these multi-band effects. This concept has been used before to indicate band convergence: for example, in PbTe, where the L and Σ bands are converged the effective degeneracy is thought to be ≈ 16 [16, 18]. Beyond cases where well-defined, individual charge carrier pockets exist, additional enhancements to thermoelectric performance can occur as a result of non-trivial topological features.

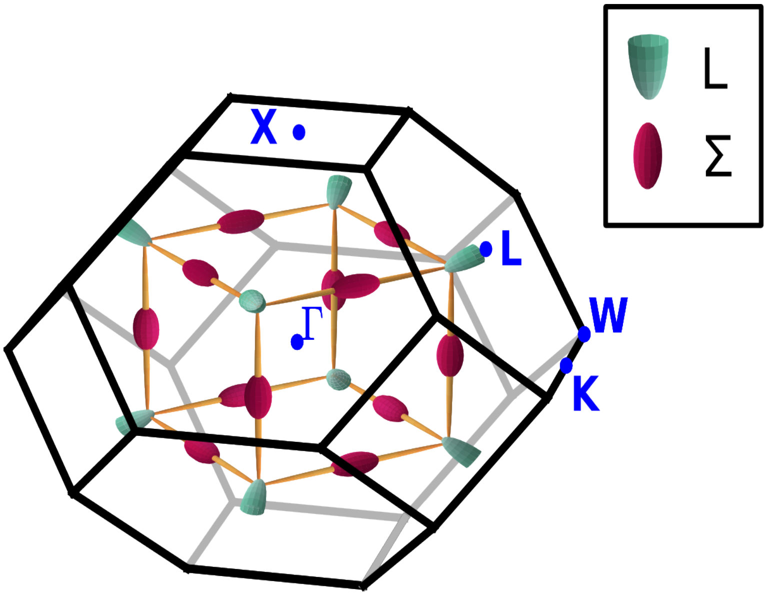

Figure 7-1: Fermi surfaces in p-type PbTe a) showing the separate ellipsoids of the L and Σ bands (leading to an increase in Nv) and b) showing the more complex Fermi surface once both the L and Σ bands have been reached, which leads to an increase in K*.*

7.2b - Effective Anisotropy Factor (K^*)

The single parabolic band model (SPB model) has an electron energy dispersion given by $E = \frac{\hbar^2 k^2}{2m^*}$, where *k* is the electron wave vector. The common definition for the effective mass is defined by the curvature of the band in k-space $m^* = \hbar^2 \left(\frac{d^2E}{dk^2}\right)^{-1}$ (light bands have high curvature, heavy bands have shallow). However, real systems often show deviations from the single parabolic band case and require a more complicated description (possibly anisotropic Fermi surfaces, non-parabolic bands, as shown in Chapters 3,4, and 6, multiple valley contributions, and/or more complicated topological features), and the band curvature definition of effective mass is not necessarily applicable nor does it even display the expected trend for the property of interest for systems that display these complex features.

In terms of Fermi surface anisotropy, only in the simplest cases can Fermi surfaces can be described as spherical pockets; many materials contain more complicated Fermi surfaces. The next level of complexity involves ellipsoidally shaped pockets where the anisotropy parameter,

$K = \frac{m_{\parallel}^*}{m_{\perp}^*}$, quantifies the degree of anisotropy. Many systems show Fermi surface anisotropy both experimentally and theoretically, such as Si/Ge [55, 56], IV-VI materials [58, 59, 360], III-V materials [57], and others [61]. The conductivity effective mass (which is a single valley harmonic average along each direction): $m_c^* = 3\left({m_{\parallel}^*}^{-1} + 2{m_{\perp}^*}^{-1}\right)^{-1}$ determines the carrier mobility ($\mu = \frac{e\tau}{m_c^*}$). m_c^* is equal to the m_b^* (geometric average: $m_b^* = \left(m_{\parallel}^* {m_{\perp}^*}^2\right)^{1/3}$) for spherical pockets ($K = \frac{m_{\parallel}^*}{m_{\perp}^*} = 1$), although in general they are different. For ellipsoidally shaped Fermi surfaces ($K \neq 1$), the effective anisotropy K^* parameter can be expressed as:

$$\boldsymbol{K^*} = \left(\frac{\boldsymbol{m_b^*}}{\boldsymbol{m_c^*}}\right)^{3/2} = \frac{(\boldsymbol{2K+1})^{3/2}}{\boldsymbol{3^{3/2}K}} \qquad \text{Equation 7-1}$$

If the density of states mass is held constant, increasing *K* (and *K**) is good for thermoelectrics because it implies that the conductivity mass would decrease (corresponding to an increased mobility and conductivity). While anisotropy is generally beneficial, some Fermi surface anisotropy cannot be captured by simply considering ellipsoidally shaped carrier pockets.

The ellipsoidal description of the Fermi surface works well in many cases, and it is easily extendible to systems with N_v>1 (or to systems with a Fermi-level dependent effective valley degeneracy, N_v^*). However, some materials exhibit additional non-trivial topological features in their Fermi surface which cannot be accounted for in the ellipsoidal framework. For example, in PbTe, once the Fermi level becomes sufficiently degenerate, narrow threads are calculated to connect the individual L and Σ bands, which results in an increasingly complex Fermi surface (as illustrated by the orange features in Figure 7-1b) [294, 295]. In cases where the Fermi surface has additional complexity, simply estimating the N_v^* is not sufficient to capture the potential enhancement to the thermoelectric quality factor, requiring the introduction of “the effective anisotropy factor”, *K**, which can be expressed explicitly for ellipsoidally shaped pockets (Equation 7-1) but must be computed from the electronic structure in general. Recent work from several groups has shown that additional thermoelectric enhancement can occur as a result of Fermi surface complexity beyond simple spherically shaped, isolated pockets in the valence bands of both IV-VI [59, 294, 295] compounds and Si [361] (and perhaps other group IV or III-V materials with similar valence band structures). This can occur as a result of oddly shaped topological features such as threads (Figure 7-1) [294] or warping resulting from multiple extrema with drastically different masses [59].

7.2c - Fermi Surface Area to Volume Ratio

While Parker et al. have attributed topological enhancements to thermoelectric performance in the IV-VI systems to low dimensional Fermi-surface features, I propose an alternative explanation involving the Fermi surface area to volume ratio. If we consider the Boltzmann transport equation:

$$\boldsymbol{\sigma_{ij} = \int_{BZ} \left(-\frac{df}{dE}\right) v_i v_j \tau(k) d^3k = \int_{BZ} \left(-\frac{df}{dE}\right) v_i v_j \tau A_k \frac{dE}{dE/dk}} \qquad \text{Equation 7-2}$$

where *f* is the Fermi distribution function, v_i is the electron group velocity (in the i^{th} direction), τ is the scattering time, *k* is proportional to the electron momentum, *E* is the electron energy, and A_k is the Fermi surface area (derived by simply substituting $d^3k = dV_k = A_k dk$ where *V* is the volume of the Fermi surface). In the usual, energy-dependent, form of the Boltzmann transport equation, the density of states is substituted $D(E) = \frac{dn}{dE} = \frac{1}{(2\pi)^3}\frac{dV}{dE} = \frac{1}{(2\pi)^3} A_k \frac{dE}{dE/dk}$. However, this form allows us to see that the in the degenerate limit (i.e., where $(-\frac{df}{dE}) \approx \delta(E - E_F)$) the electrical conductivity is simply proportional to the Fermi surface area.

If we can also consider the carrier concentration:

$$\boldsymbol{n} = \frac{\boldsymbol{V_k}}{(\boldsymbol{2\pi})^3}$$ Equation 7-3

which is simply equal to the volume enclosed by the Fermi surface divided by the volume of a single *k*-point (which the particle in a box model states is $\left(\frac{2\pi}{L^*}\right)^2$, where L^* is the sample dimension). The ratio of the electronic conductivity to the carrier concentration gives a value proportional to the mobility; therefore, mobility is increased if the surface area to volume ratio of the Fermi surface is large, as is the case for many complex Fermi surface features (such as the threads in Figure 7-1). This effect will benefit zT by allowing a larger electronic conductivity without drastically altering the Fermi level. Recent work by Pei et al. shows that low effective mass (i.e., high mobility) is desirable for thermoelectric band engineering, contrary to popular opinion which suggests high mass is good [106]. I believe that these complex topological features likely produce high quality factors owing to their large surface area to volume ratios, and that in the case where appreciable amounts of carriers exist in these states, they can contribute significantly to zT.

7.2d - Fermi Surface Complexity Factor ($N_v^* K^*$)

In this thesis chapter, I will attempt to describe the effects of valley degeneracy (and more broadly Fermi surface complexity) with a single parameter which we will call the “Fermi surface complexity factor”, $(N_v^* K^*)$. I define the “Fermi surface complexity factor” as $(N_v^* K^*) = \left(\frac{m_S^*}{m_c^*}\right)^{3/2}$ where the conductivity mass, m_c^*, and m_S^* is the effective mass obtained from Seebeck coefficient and carrier concentration using the SPB model. These two parameters are simply estimated from outputted Boltztrap calculation results and reflect parameters that are observed directly in the thermoelectric quality factor. Using transport properties estimated from the Boltztrap code in conjunction with the calculated band structure properties, we show how to obtain a chemical potential dependent estimate of $(N_v^* K^*)$ for any compound that does not depend on the assumed scattering mechanism. We apply this technique across a large number of materials from the Materials Project high-throughput thermoelectric properties database to validate the theory.

Single Parabolic Band Model from Boltztrap (m_S^*)

Calculated Boltztrap data will be analyzed in the context of the Seebeck Pisarenko plot (*S* vs *n*), which is commonly used when analyzing experimental data. Using the Pisarenko plot, the data can easily be understood in the context of a single parabolic band model (also assuming constant scattering time) with the relevant fitting parameter being the effective mass (m_d^*). The equations are shown for the thermoelectric parameters as a function of the reduced chemical potential: $\eta = \frac{\xi}{k_B T}$ are shown below for an arbitrary power law dependence of the scattering time $\tau(\epsilon) = \tau_0 \epsilon^{\lambda - 1/2}$ ($\lambda = 1/2$ for constant scattering time as is assumed in Boltztrap) [24]:

$$\boldsymbol{S(\eta) = \frac{k_B}{e}\left[\frac{(2+\lambda)}{(1+\lambda)}\frac{F_{1+\lambda}(\eta)}{F_\lambda(\eta)} - \eta\right]} \qquad \text{Equation 7-4}$$

$$\boldsymbol{n(\eta) = \frac{1}{2\pi^2}\left(\frac{2m_d^* k_B T}{\hbar^2}\right)^{\frac{3}{2}} F_{1/2}(\eta)} \qquad \text{Equation 7-5}$$

where λ determines the scattering exponent, n is the charge carrier concentration, and m_d^* is the density of states effective mass. The effective mass can be determined using experimental parameters by supplying a measured Seebeck coefficient and *n* and solving for both η and m_d^*. This method can also be applied to calculated Boltztrap data (*S* vs *n*) to get an estimate for m_d^*, which we will call m_S^* (effective mass from Seebeck coefficient).

Boltztrap Conductivity Mass (m_c^*)

The conductivity effective mass is calculated directly from Boltztrap data by considering the electrical conductivity, σ. Boltztrap estimates the conductivity tensor (divided by τ) by solving the Boltzmann transport equation (Equation 7-2) for a given calculated electronic structure and temperature. The conductivity effective mass tensor can be calculated as $\boldsymbol{m}_{\boldsymbol{c}}^{*} = ne^{2}(\boldsymbol{\sigma}/\tau)^{-1}$, where *n* is the carrier concentration, *e* is the fundamental electron charge, and $\boldsymbol{\sigma}/\tau$ is the conductivity tensor divided by the scattering time. Interestingly, because Boltztrap computes the ratio of the conductivity tensor to the scattering time ($\boldsymbol{\sigma}/\tau$), the conductivity mass tensor ($\boldsymbol{m}_{\boldsymbol{c}}^{*}$) should represent the band structure and should not depend on the scattering time. One complaint about Boltztrap thermoelectric transport results is that they use the CRTA, which we know to not be valid for most experimental systems that show APS. By computing m_{S}^{*} and $\boldsymbol{m}_{\boldsymbol{c}}^{*}$, which presumably do not depend on scattering, we hope to improve the applicability of the Boltztrap method to experimental results, especially in the context of band engineering, effective valley degeneracy (N_{v}^{*}), and effective anisotropy factor (K^{*}).

7.3 - Results and Discussion

7.3a - III-V Materials

N_{v}^{*}, the effective valley degeneracy, can be described as the number of valleys which conduct in parallel. In the case where only a single carrier pocket participates in conduction (not considering symmetry), $N_{v}^{*} = N_{v}$. Many real semiconducting systems have multiple band extrema within 1.0 eV of the band edge, implying that a Fermi-level dependent effective valley degeneracy should be defined which more accurately represents the changing number of degenerate pockets. N_{v}^{*} would reflect a smooth transition from one value of N_v to another as the carrier density the secondary pocket increases; this can be compared to the step-change in N_v that might be expected as the energy of the secondary band is reached just by considering the symmetry of the extrema alone (green line in Figure 7-2a, $N_{v}(E_{F}) = \sum N_{v,i}\mathrm{H}(E_{F} - E_{i})$ where H is the Heaviside step function and E_i is the energy of the i^{th} band extrema). As the first example of where the Fermi surface complexity factor is applied, we have considered AlAs, shown in Figure 7-2.

The calculated DFT electronic band structure and Boltztrap data analyzed using the $(N_v^* K^*)$ method (Materials Project, mp-2172) for AlAs are shown in Figure 7-2 along with the true valley degeneracy (N_v) computed directly from the band extrema positions and the Brillouin zone symmetry. The primary conduction band minimum occurs at the X-point ($X_{\text{-c}}$ N_v=3), which agrees with the computed $(N_v^* K^*) = 3.5$ within the band gap near the conduction band edge. As the Fermi level moves into the conduction band, we reach the Γ_{-c} (N_v=1, 0.28 eV above $X_{\text{-c}}$) and $L_{\text{-c}}$ (N_v=4, 0.51 eV above $X_{\text{-c}}$) bands, the actual N_v increases to 4 and 8, respectively. The Fermi surface complexity factor $(N_v^* K^*)$ increases steadily from the band edge resulting in a value of 3.5 and 6.1 at the Γ_{-c} and $L_{\text{-c}}$ band edge energies, respectively. $(N_v^* K^*)$ continues to increase reaching a maximum value of ~12.5. This is not quite as high as one might expect based on the high degeneracy of the K_{-c} extrema (N_v=12, 0.75 eV below $X_{\text{-c}}$) or the additional $X_{2\text{-}c}$ band (N_v=3, 0.78 eV below X_{-c}). It is not readily apparent why the full 23 valleys are not observed through $(N_v^* K^*)$, but it could be related to the fact that the thermopower is quite low (less than 20 μV/K) for these Fermi levels, meaning that we may be reaching the limit of the calculation resolution. Up until high energies, though, the thermoelectric Fermi surface complexity factor $(N_v^* K^*)$ seems to mirror the true N_v both qualitatively and quantitatively—indicating an anisotropy component, K^*, that is likely near unity.

If we consider the valence band of AlAs, it, like all of the III-V materials calculated in this chapter, consists of three degenerate bands, $\mathit{\Gamma}_{1,2,3-\text{v}}$, each of which vary significantly in effective mass (light hole, heavy hole, and split-off band). As a result, the Fermi surface, even though it is centered at the $\mathit{\Gamma}$ point, will have a non-trivial topology (as suggested by Mecholsky et al. for silicon [361]), which will result in a larger K^* component to the Fermi surface complexity factor. For the valence band, $(N_v^* K^*) = 9$, which is an overestimate relative to the expected degeneracy of N_v=3 for $\Gamma_{1,2,3-v}$. Mecholsky et al. shows that the warped Fermi surfaces, which result from the combination of light and heavy holes in silicon, lead to interesting consequences for the effective mass and conductivities in these systems [361], consistent with inflated $(N_v^* K^*)$ observed for $\Gamma_{1,2,3-v}$ here.

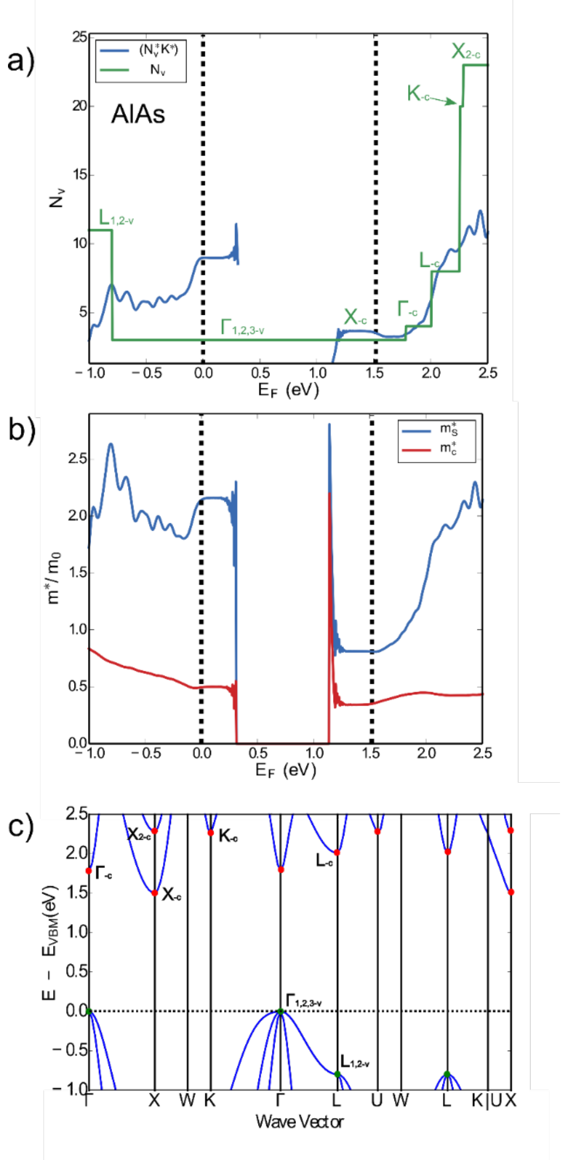

Figure 7-2: Boltztrap (300 K) and band structure calculation results for AlAs. a) "Fermi surface complexity factor" and true valley degeneracy plotted as functions of the Fermi level across the valence and conduction band. b) The conductivity (m_c^*) and density of states (as estimated from Seebeck coefficient, m_S^*) effective masses plotted as a function of Fermi energy. c) Band structure calculation results for AlAs with the near-edge extrema indicated and labelled.

Upon calculating the Fermi surface complexity factor for other III-V compounds, we can see many analogs to the AlAs results. AlP (Figure 7-3a) shows a primary extrema at $X_{\text{-}c}$ (N_v=3), which $(N_v^* K^*)$ matches well; this is followed by the $K_{\text{-}c}$ (N_v=12, at 0.83 eV above $X_{\text{-}c}$) and $X_{2\text{-}c}$

(N_v=3, at 0.85 eV above X_{-c}) bands, which result in a small increase in $(N_v^* K^*)$ up to >10.0 (although not until ~1.2 eV above X_{-c} edge, which is not plotted). The conduction band of AlSb in Figure 7-3b shows three near-converged bands with the primary L_{-c} band (N_v=4) accompanied by a $(\Gamma - X)_{-c}$ (N_v=6 at 0.03 eV above L_{-c}) and Γ_{-c} (N_v=1 at 0.05 eV above L_{-c}). Because these two bands are so close in energy (within 2 $k_B T$ at 300 K) to the conduction band edge, it is not surprising that $(N_v^* K^*)$ more closely reflects the sum of the degeneracy for these bands; even within the band gap, $(N_v^* K^*) \approx 14$. This value is slightly larger than the expected N_v of 11, but it is possible that the nearby X_{-c} band with N_v=3 could also be contributing as well. The conduction bands of GaN and GaSb are a bit simpler in that their primary conduction band lays at Γ_{-c}, resulting in both yielding $(N_v^* K^*) \approx 1$, as expected. In the case of GaAs, a secondary band at L_{-c} (N_v=4, at 0.69 eV above Γ_{-c}) results in an abrupt jump in the Fermi surface complexity factor up to about 7.0 around this energy. The details of each of the n-type III-V compounds' effective masses, expected valley degeneracy, and Fermi surface complexity factors are included in Table 7-3. The valence bands of all of the III-V compounds in this work showed the same triply degenerate at the $\Gamma_{1,2,3-v}$ behavior as in AlAs (Figure 7-2c), some were followed by a doubly degenerate at L_{12-v}; however, the L_{12-v} extrema were usually much lower in energy and did not effect $(N_v^* K^*)$ much. In all cases, $(N_v^* K^*)$ was between 6 and 10 at the valence band edge ($\Gamma_{1,2,3-v}$), which is greater than the expected N_v of 3.0, which should be attributed to the effective anisotropy factor (K^*) as mentioned previously for AlAs.

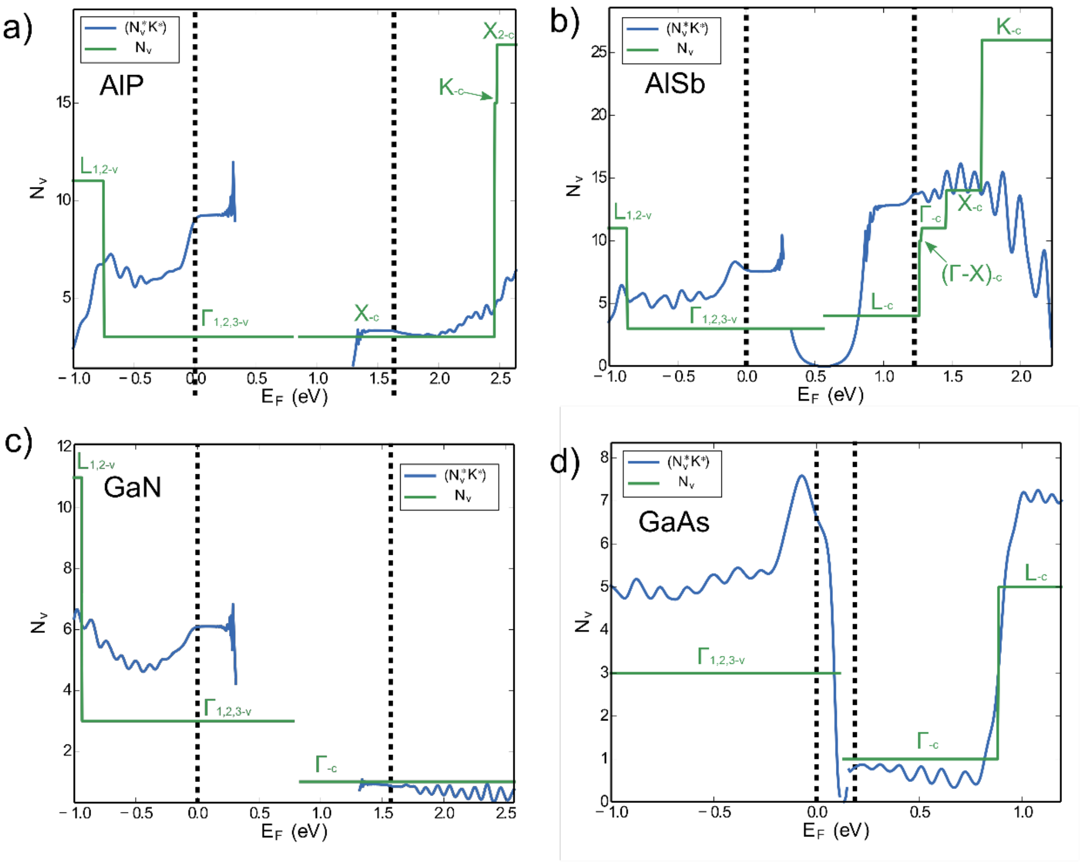

Figure 7-3: Fermi surface complexity factor computed for several III-V compounds along with their expected valley degeneracies for a) AlP (mp-1550), b) AlSb (mp-2624), c) GaN (mp-830, Zinc Blende structure), and d) GaAs (mp-2534).

Table 7-1: III-V semiconductor results regarding their true valley degeneracy extracted from band structure (CBM Loc, CB Deg), and their conductivity/Seebeck effective masses and Fermi surface complexity factors computed at the energy of the contributing band. E_g (band gap) is in eV, and MPID corresponds to the mp-id parameter used to store data within the Materials Project (materialsproject.org).

	MPID	E_g	CBM Loc	CB Deg	m_s^*	m_c^*	$N_v^*K^*$
AlN	1700	3.31	X, Γ(0.69)	3, 1	0.81, 0.96	0.39, 0.47	3.0, 3.0
AlP	1550	1.63	X, K (0.83), X (0.85)	3, 12, 3	0.77, 1.39, 1.46	0.35, 0.51, 0.51	3.3, 4.5, 4.9
AlAs	2172	1.5	X, Γ (0.28), L (0.51), K (0.75), X (0.78)	3, 1, 4, 12, 3	0.81, 0.97, 1.49, 1.94, 2.00	0.35, 0.42, 0.45, 0.42, 0.42	3.6, 3.5, 6.1, 9.8, 10.2
AlSb	2624	1.23	L, Γ-X (0.03), Γ (0.05), X (0.23), K (0.49)	4, 6, 1, 3, 12	1.37, 1.49, 1.53, 2.01, 2.05	0.24, 0.26, 0.27, 0.32, 0.36	13.7, 13.8, 13.9, 15.5, 13.7
GaN	830	1.57	Γ	1	0.15	0.16	0.9

GaP	2490	1.59	L, Γ (0.00), Γ-X (0.05), X (0.26), K (0.63)	4, 1, 6, 3, 12	1.23, 1.23, 1.40, 1.93, 2.08	0.22, 0.22, 0.24, 0.33, 0.39	13.0, 13.0, 14.1, 14.2, 12.3
GaAs	2534	0.19	Γ, L (0.69)	1, 4	0.03, 0.25	0.04, 0.12	0.8, 3.1
GaSb	1156	0	Γ, L (0.32), Γ-X (0.93)	1, 4, 6	0.02, 0.24, 0.89	0.03, 0.09, 0.22	0.5, 4.7, 8.4
InN	20411	0	Γ	1	0.09	0.12	0.66
InP	20351	0.47	Γ, L (0.93)	1, 4	0.055, 0.47	0.06, 0.27	0.84, 2.6
InAs	20305	0	Γ, L (0.84)	1, 4	0.03, 0.43	0.05, 0.24	0.6, 2.4
InSb	20012	0	Γ, L (0.44)	1, 4	0.03, 0.31	0.05, 0.13	0.5, 3.5

7.3b - IV-VI Materials – The Lead Chalcogenides

As mentioned previously (Chapter 4), the lead chalcogenides (including PbSe [65, 261], PbS [13], and their alloys [12, 19, 25, 121, 362-366]) are known to be good thermoelectric materials. Much of this is attributed to their high valley degeneracy resulting from an accessible Σ_{-v} band. I have applied the Fermi surface complexity factor analysis to both PbSe and PbS, the results of which are shown in Figure 7-4. The Σ_{-v} band lays 0.34 and 0.48 eV below L_{-v} in PbSe and PbS, respectively (which agree with previous experiment [25, 261, 367] and theory [25, 126, 294]); the computed band offsets, expected valley degeneracies, and observed $(N_v^* K^*)$ are tabulated in Table 7-4. Both PbSe and PbS show good agreement with the expected N_v of 4 for both the conduction and valence bands within the band gap. As the Fermi level moves deeper into the valence band, the Σ_{-v} results in a peak in $(N_v^* K^*)$ of ~19 and 14 for PbSe and PbS, respectively (close to the expected value of 16). Additional extrema at the W_{-v} (and $(\Gamma - X)_{-v}$ in the case of PbSe) result in another large peak in $(N_v^* K^*)$ up to values of ~41 (at 0.75 eV below L_{-v}) and ~16 (at 0.94 eV below L_{-v}) for PbSe and PbS, respectively. Each of the peak values agrees qualitatively with the expected N_v from band structure, although $(N_v^* K^*)$ is higher than expected for the $W_{-v}/(\Gamma - X)_{-v}$ in PbSe, implying that $K^*>1$. K^* is likely larger due to non-trivial topological features that are well-known to occur in the valence band of the lead chalcogenides beginning below the Σ_{-v} band (as mentioned in a previous section and shown schematically in Figure 7-1) [121, 294, 295]. For PbSe and PbS, the conduction band only shows some deviations from $(N_v^* K^*) = 4$ within the gap as expected from the primary conduction band, L_{-c}, but they do show some increase as the secondary conduction band (Σ_{-c}) arises at 0.79 and 0.88 eV above the band edge, respectively (although the value does not reach the expected value of N_v=16).

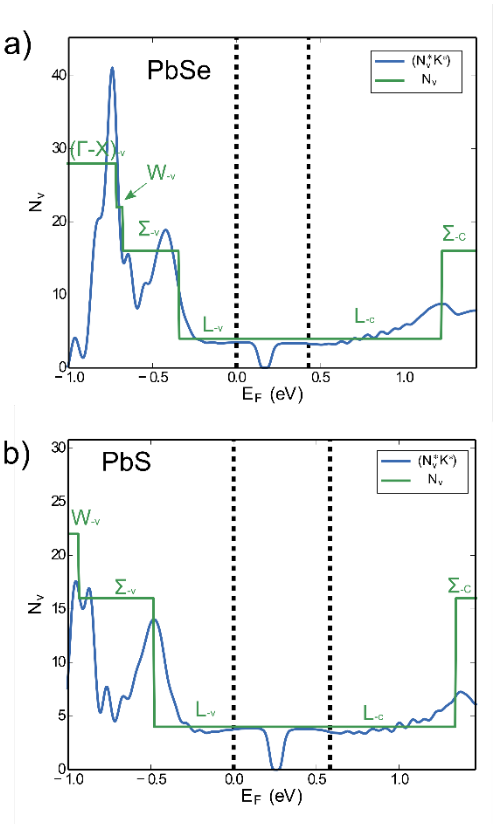

Figure 7-4: The Fermi surface anisotropy factor and valley degeneracy plotted for a) PbSe (mp-2201) and b) PbS (mp-21276).

Table 7-2: Valence band parameters for several IV-VI materials of thermoelectric interest. Band gaps (E_g) is listed in eV. VBM locations are given by their position in k-space (which also corresponds to Figure 7-5 and Figure 7-4) as well as their energy offset relative to the valence band edge. We have included their degeneracy (individual band degeneracy, not cumulative, which is plotted in Figure 7-4a), the Seebeck/conductivity effective mass (m_c^*, m_{Seeb}^*), and the calculated effective valley degeneracy, N_v^*, at each corresponding band edge energy. For SnTe, which had a very low band gap, values for the L band were taken 0.1 eV below the band edge so as to avoid strong bipolar effects.

	MPID	E_g	VBM Loc	VBM N_v	m^*_{Seeb}	m^*_c	N_v^*
PbTe	19717	0.81	L, Σ (0.12), Γ-X (0.30), W (0.30), Σ_2 (0.64), $L_{2,3}$ (0.76)	4, 12, 6, 6, 12, 4x2	0.71, 2.29, 4.82, 1.37, 1.78	0.17, 0.23, 0.33, 0.41, 0.45	8.7, 30.8, 56.9, 6.0, 7.9
PbSe	20667	0.43	L, Σ (0.34), W (0.68), Γ-X (0.72)	4, 12, 6, 6	0.37, 1.49, 2.87, 5.22	0.16, 0.30, 0.47, 0.49	3.5, 11.1, 14.9, 34.6
PbS	21276	0.46	L, Σ (0.48), W (0.94), Γ-X (1.00)	4, 12, 6, 6	0.48, 2.19, 4.13, 2.69	0.20, 0.38, 0.63, 0.62	3.8, 14.0, 16.9, 9.0

SnTe	1883	0.04	L, Σ (0.36), Γ-X (0.80), W (0.82)	4, 12, 6, 6	0.16, 1.13, 2.58, 3.16	0.07, 0.15, 0.32, 0.32	3.6, 21.7, 22.4, 30.7

Of the lead chalcogenides, PbTe has been shown to yield the best thermoelectric performance. Experimentally, p-type PbTe stands out from PbSe and PbS mainly due to its relatively small band offset between the L_{-v} and Σ_{-v} bands and lower thermal conductivity [16, 123-126, 162]. Figure 7-5 shows the computed band structure, the Fermi surface complexity factor $(N_v^* K^*)$, and computed effective masses for PbTe. Figure 7-5c shows the large number of near-edge bands that exist in PbTe in both the valence and conduction band. I show the calculated $(N_v^* K^*)$ along with the expected valley degeneracy contributions for the different extrema (Figure 7-5a). Upon the Fermi level entering the valence band, we observe an $(N_v^* K^*)$ of ~9, which continues to increase as the Fermi level moves further into the band. While in the case of PbSe and PbS $(N_v^* K^*) \approx N_v(L_{-v}) = 4$ within the gap near the L_{-v} edge, PbTe shows a larger band edge Fermi surface complexity factor. It is not clear whether this is due to some influence of the Σ_{-v} band (which is computed to be only ~0.12 eV or 4.8 k_BT at 300 K away from L_{-v}), which would imply N_v^*>4, or whether it may be due to the fact that the L_{-v} bands for PbTe are more ellipsoidal (K^*>1) than in PbSe and PbS (observed in the literature [58, 59, 360].) As E_F moves further into the valence band, we can see a rapid increase in m_S^* (Figure 7-5b) because of the additional influence of the high degeneracy Σ_{-v} band. Despite the large increase in m_S^*, the conductivity mass increases only modestly, resulting in a rapid increase in $(N_v^* K^*)$. Once the Fermi level reaches the Σ_{-v} band, $(N_v^* K^*)$ reaches values near 30, much greater than the expected N_v of 16. The Fermi surface complexity factor continues to increase rapidly as we reach the W_{-v}, $(\Gamma - X)_{-v}$, Σ_{2-v}, and $L_{2,3-v}$ at 0.3, 0.3, 0.64, 0.76 eV below L_{-v}, respectively, ultimately achieving an extremely large value around 60. While a large N_v is expected from the many valence bands (reaching a value of ~50, green line Figure 7-5a), $(N_v^* K^*)$ rises very quickly and reaches a peak value that is much higher than expected (from the actual N_v). It is clear that $(N_v^* K^*)$ cannot be explained by simply considering N_v^* alone, implying that K^*>1. As mentioned previously, it is well-known that the lead chalcogenides exhibit a complicated Fermi surface that involves a merging of the separate pockets (L_{-v} and Σ_{-v}) [59, 121, 294, 295], which is likely causing the large K^* value (threads shown in Figure 7-1). As mentioned in the theory section, recent work from Parker et al. suggests that cylindrical "threads" that connect the L_{-v} and Σ_{-v} pockets result in a significantly larger Fermi surface area, which is suggested to benefit thermoelectric properties [295]. While Parker et al. attribute this to a reduced-dimensional Fermi surface, my explanation involves the large surface area to volume ratio of the states which these charge carriers occupy; this results in these thread-like states having an inherently large mobility and quality factor (and corresponding large K^*).

The conduction band also benefits from a large number of additional carrier pockets with high degeneracy. A corresponding analog of the Σ_{-v} valence band is calculated to exist in the conduction band (Σ_{-c}) at ~0.54 eV above the band edge. This band is accompanied by a doubly degenerate *L*-band ($L_{2,3-c}$). Each of these bands increase ($N_v^* K^*$), resulting in a peak around this energy. It is important to note that experimentally in *n*-type PbTe, it is difficult to dope to high enough carrier concentration to reach any secondary conduction bands [28]; Boltztrap calculations suggest that carrier concentrations of >$2 \times 10^{21}\ cm^{-3}$ to reach the Σ_{-c} band (whereas experimentally, the maximum attainable n_H has been shown to be an order of magnitude less [28]).

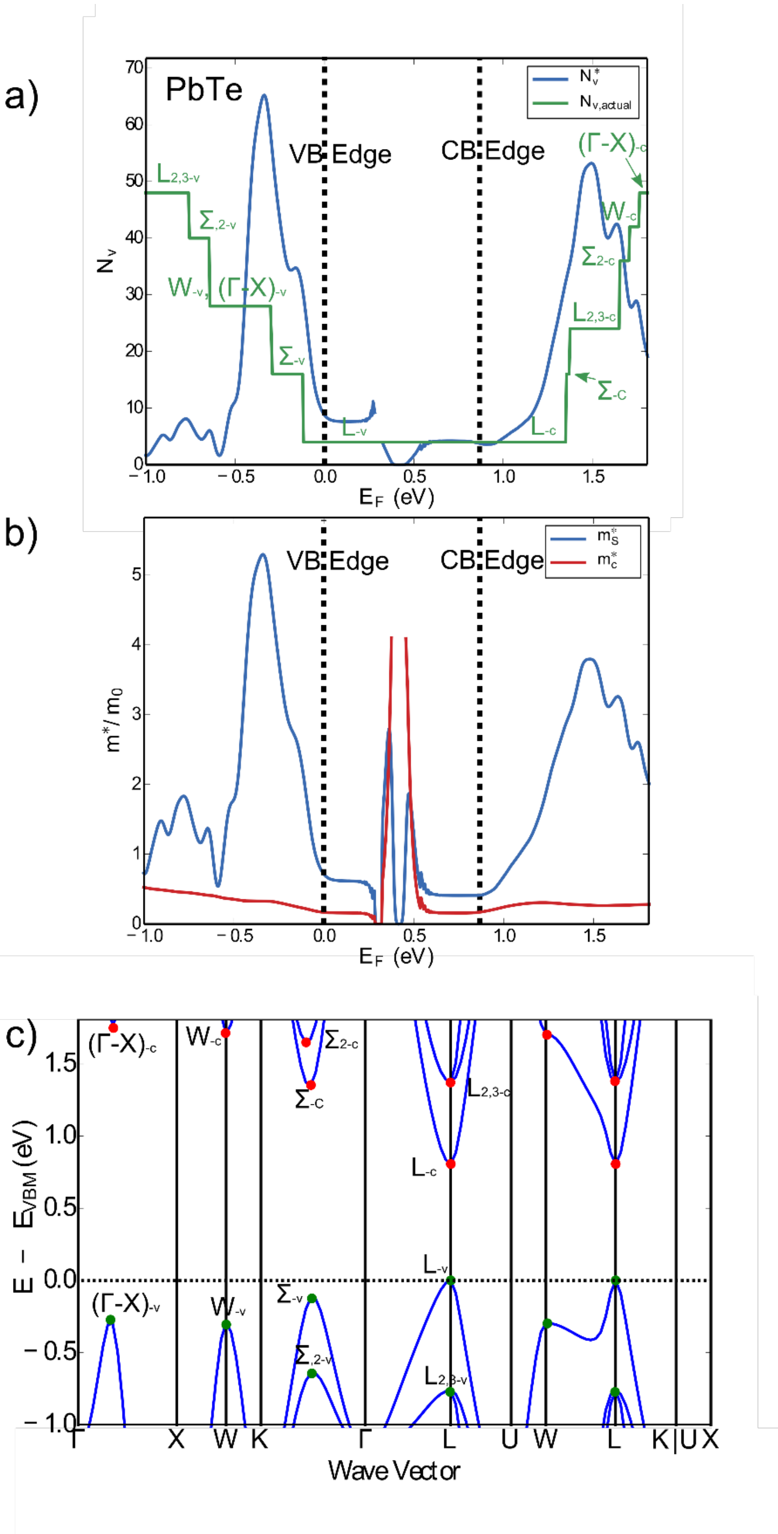

Figure 7-5: PbTe (mp-19717) calculated results for a) effective valley degeneracy (N_v^*), b) density of states (m^*_S), and conductivity effective mass (m^*_c), as well as the near-edge band structure including the marked and labeled band extrema. The valence and conduction band edge is shown in a,b, as a dashed line (anything between the dashed lines exists within the band gap). c) The computed electronic structure of PbTe with the extrema indicated.

7.3c - High Throughput Computation

The thermoelectric quality factor (*B*) which scales both the maximum carrier concentration dependent power factor and *zT* is well-known for the acoustic phonon scattering regime (Equation 2-6, the most commonly observed experimental scattering mechanism for thermoelectric materials at T>300 K) as outlined in the introduction of this chapter. While acoustic phonon scattering is the most common scattering mechanism for high temperature materials, constant scattering time (CRTA) is simpler to implement from a computational perspective (in Boltztrap) and is very commonly used to gauge a material's thermoelectric performance directly from *ab-initio* calculations. Here, the thermoelectric quality factor can be derived as:

$$\begin{aligned}\mathbf{B}_{\tau=\text{constant}} &= \frac{\mathbf{k}_\mathbf{B}^{7/2}2^{3/2}}{3\pi^2\hbar^3}\left(\frac{\mathbf{m}_\mathbf{d}^{*\,3/2}}{\mathbf{m}_\mathbf{c}^*}\right)\frac{\tau}{\kappa_\mathbf{L}}\mathbf{T}^{5/2} \\ &= \frac{\mathbf{k}_\mathbf{B}^{7/2}2^{3/2}}{3\pi^2\hbar^3}\frac{(\mathbf{N}_\mathbf{v}^*\mathbf{K}^*)^{2/3}\mathbf{m}_\mathbf{d}^{*\,1/2}\tau}{\kappa_\mathbf{L}}\mathbf{T}^{5/2}\end{aligned} \qquad \text{Equation 7-6}$$

For constant scattering time, $B_{\tau=constant} \propto (N_v^* K^*)^{2/3} {m_d^*}^{1/2}$, indicating that systems with higher effective mass will lead to a higher predicted power factor and *zT* from Boltztrap calculations. The result is qualitatively different than B_{APS}, which yields an inverse effective mass dependence proportional to $\frac{N_v}{m_c^*}$ (or $\frac{(N_v^* K^*)}{m_b^*} = \frac{N_v^*}{m_c^*}$); this implies that light mass, high mobility materials with high valley degeneracy are the best for thermoelectrics [106]. We propose the "Fermi surface complexity factor" $(N_v^* K^*)$ as a better predictor of thermoelectric performance than Boltztrap computed Seebeck coefficient or power factor because it scales directly with thermoelectric quality factor in both the APS and CRTA cases. Further, $(N_v^* K^*)$ links the desired thermoelectric quantities (*B*, conductivity, Seebeck coefficient) directly to the computed electronic band structure, specifically through the valley degeneracy and effective anisotropy. Also, it captures the effects that complex Fermi surfaces can have on the thermoelectric performance through *K**.

The vast electronic structure database constructed through the Materials Project allows for large-scale screening of thermoelectric materials using Boltztrap (using the CRTA). Figure 7-6 shows the correlation between $(N_v^* K^*)$ and the calculated maximum (Fermi level-dependent) power factor for the large group of compounds (~2300 isotropic compounds) assuming a specific scattering time ($\tau = 1 \times 10^{-14}\ s$) at 600 K. We can see a good correlation between the calculated Fermi surface complexity factor and the maximum attainable power factor; this is expected since the quality factor for constant relaxation time is expected to scale as $B_{\tau=constant} \propto (N_v^* K^*)^{2/3}$. The line on Figure 7-6 indicates a 2/3 power slope, which is expressed well for the dataset.

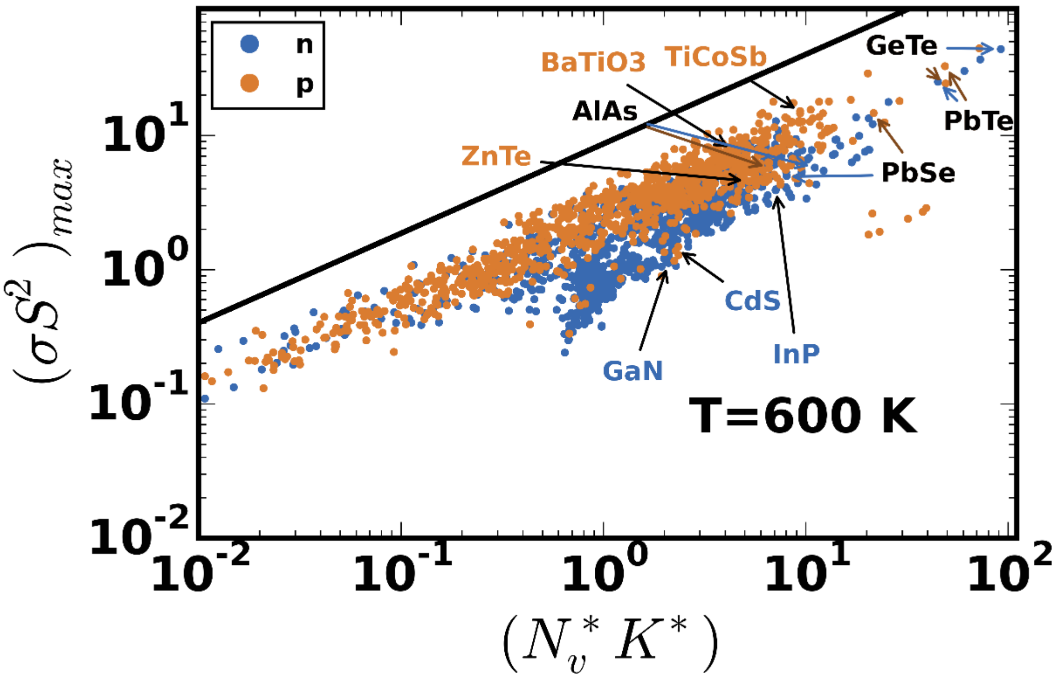

Figure 7-6: Maximum power factor for ~2300 cubic compounds plotted as a function of the Fermi surface complexity factor (evalulated at the Fermi level that yields the maximum power factor) at T=600 K).

7.4 - Conclusions

I have introduced and examined the Fermi surface complexity factor $(N_v^* K^*)$ and its relation to the valley degeneracy. I have conceptually separated the components of the Fermi surface complexity factor into the effective valley degeneracy (N_v^*) and the effective anisotropy factor (K^*) by examining several known material systems (III-V and IV-VI semiconductors). We infer that the valence bands in both the III-V and IV-VI have a larger than expected Fermi surface complexity factor which exceeds the expected degeneracy, likely as a result of non-trivial topological features which enhance K^*. We have also shown that ($N_v^*K^*$) should not depend on the particular scattering time assumptions, making results from it more consistent with experimental observations that tend to exhibit acoustic phonon scattering. We have analyzed the maximum power factors and zT's for a large set (>2300) cubic compounds from the Materials Project to show that ($N_v^*K^*$) seems to correlate well with both the maximum power factor (and also the quality factor). Correlation of experiments and theory is of critical importance both for validating theoretical calculations and for interpretation of experimental results. High throughput Boltztrap calculations have the potential for high-impact in the community for their predictive power, by understanding these calculated properties in the context of band engineering they can have an even broader use.

7.5 - Methods

Ab-initio computations in this section are from the Materials Project database [368] and use DFT within the generalized gradient approximation (GGA) in the Perdew-Burke-Ernzheroff (PBE) formulation [336]. Calculations were performed using the VASP software and projector augmented-wave pseudopotentials [369]. Bolztrap calculations were computed using the open-source code [30] along with analysis and plotting software from pymatgen [370].

When considering the IV-VI materials, all materials are calculated in their most stable configuration (unit cells relaxed in the rock salt—space group 225—structure). In PbTe in particular, the calculated band gap from GGA is much larger than the experimental band gap (~0.3 eV at 300K for PbTe [126]). Literature suggests that if spin-orbit coupling (SOC) was considered, the gap shrinks to near the experimental values [85]; however, we have neglected SOC contributions in this work. Regardless, because Boltztrap calculations are done at T=300 K, the band gap itself should not greatly affect the results; the results would be affected most for Fermi levels within the band gap, which is not where the interesting valley degeneracy effects occur. The effect is also present in PbSe and PbS, although to a lesser extent.

Specifically considering the III-V materials, we have assumed that each is crystallized in the zinc-blende crystal structure (Space group 216), even though the nitrides are more stable in the hexagonal Wurtzite structure [57, 371]. We also should point out that standard DFT calculations do not always provide the correct ordering of the conduction band minima (at the L, X, Γ, and K points) [57, 372, 373], but for simplicity and to illustrate the effectiveness of the Fermi surface complexity factor, we have assumed that these are the correct band structures and have interpreted all of the results with that assumption in mind (Wang et al. suggest the use of the modified Becke-Johnson semilocal exchange for values that more accurately represent experimental values [373, 374]). Further, while the valence band structure is similar among all of the III-V materials (triply degenerate at the Γ point in the absence of spin-orbit coupling), we realize that if we had included spin-orbit coupling that one of the bands (the one with the intermediate effective mass) would split off from the other two (with the energy offset increasing with the mass of the elements).

High throughput calculations of the Fermi surface complexity factor are analyzed in Figure 7-6, but we limit the analysis to cubic compounds (maximum deviation in the eigenvalues of the power factor tensor of less than 3% along any direction) and those with a maximum optimum carrier concentration less than $1 \times 10^{22}\ cm^{-3}$. We also chose to remove compounds that were not particularly stable or those that were metallic (we required that the energy above the convex hull be <0.05 eV, and that the band gap be >0.03 eV).